Autoionization of Ultracold Cesium Rydberg Atom in $37D_{5/2}$ State

Yuechun Jiao [1,2,†] , Liping Hao [3,†], Jiabei Fan [1], Jingxu Bai [1], Jianming Zhao [1,2,*] and Suotang Jia [1,2]

1 State Key Laboratory of Quantum Optics and Quantum Optics Devices, Institute of Laser Spectroscopy, Shanxi University, Taiyuan 030006, China; ycjiao@sxu.edu.cn (Y.J.); 202012603004@email.sxu.edu.cn (J.F.); 202012603001@email.sxu.edu.cn (J.B.); tjia@sxu.edu.cn (S.J.)
2 Collaborative Innovation Center of Extreme Optics, Shanxi University, Taiyuan 030006, China
3 Department of Materials and Chemical Engineering, Taiyuan University, Taiyuan 030032, China; haoliping@tyu.edu.cn
* Correspondence: zhaojm@sxu.edu.cn
† These authors contributed equally to this work.

Abstract: We present the observation of an autoionization of cesium $37D_{5/2}$ Rydberg atoms in ultracold gases and analyze the autoionization mechanism. The autoionization process is investigated by varying the delay time t_D and Rydberg atomic density. The dependence of ionization signals on Rydberg density shows that the Rydberg density has an effect on not only the initial ion signals but also the evolution of the Rydberg atoms. The results reveal that the initial ionization of $37D_{5/2}$ Rydberg atoms is mostly attributed to the blackbody radiation (BBR)-induced photoionization, and the BBR-induced transitions to the nearby Rydberg states that lead to further ionization. Our work plays a significant role in investigating the collision between Rydberg atoms and many-body physics.

1. Introduction

Cold Rydberg atoms excited to excited states [1] with a large principal quantum number n are attracting significant interest due to their strong tunable interaction, which leads to a blockade effect [2,3], many-body physics [4,5], state-changing collisions [6,7], spontaneous evolution to ultracold plasmas [8,9], etc. The interaction between Rydberg atoms plays an important role in potential advanced applications such as quantum simulators [10,11], quantum information processing [12], quantum computation [13], and atomic clocks [14].

Ultracold Rydberg atoms are considered as frozen Rydberg gases [4] and they display an autoionization due to the collisions and strong interaction between Rydberg atoms. Autoionization of Rydberg atoms is a process by which a Rydberg atom loses its outermost electron due to photoionization, electron collision, and other reasons. Autoionization is related not only to the double excited state ionization of individual atoms or molecules, but also to the collision and radiation ionization of the ultracold Rydberg gas [15,16], which plays an important role in the spontaneous evolution of dense Rydberg atoms into ultracold plasmas. The ultracold Rydberg gas provides a platform to investigate the interaction between Rydberg atoms and many-body collision. Normally, the autoionization of ultracold Rydberg gases is found on time scales of μs [17]. Some processes have been identified as the possible mechanism leading to the ionization of Rydberg atoms. The first one is the blackbody radiation, which is an important process of direct photoionization for the cold Rydberg gas. The second one is the collision process in which the long-range interaction between Rydberg atoms accelerates the initial Rydberg atoms toward each other until they collide. In this process, the ionization cross section is typically very large [18,19]. Theoretical studies show that at a large Rydberg atom number, the autoionization due to the interaction between adjacent Rydberg atoms becomes an increasingly important mechanism [20].

The ionization probability can be increased in a many-particle system featuring attractive or repulsive Van der Waals interactions [15] and Rydberg-state ionization dynamics in strong electric fields have been investigated [21,22].

In this work, we investigate the autoionization process of cesium $37D_{5/2}$ Rydberg atoms in a standard magneto-optical trap (MOT). Rydberg atoms are prepared with a two-photon excitation and the free ions are detected with a microchannel plate (MCP) detector. The free ion signals and evolution dynamics as function of delay time t_D are observed. The autoionization of the Rydberg state is analyzed by changing the Rydberg atomic density and delay time t_D, and we find that the $37D_{5/2}$ autoionization signals show rapid increasing and reaching a maximum value after the threshold delay time t_0. The threshold delay time t_0 is found to be dependent on the Rydberg density.

2. Experimental Setup

In Figure 1, we present the experimental setup and relative atomic levels. Figure 1a presents the two-photon excitation diagram. The first photon, $\Omega_p = 2\pi \times 36.16$ MHz, drives the lower transition, $|6S_{1/2}, F = 4\rangle \to |6P_{3/2}, F' = 5\rangle$, and the frequency is blue shifted 360 MHz from the intermediate level $|6P_{3/2}, F' = 5\rangle$ using a double-pass acousto-optic modulator (AOM). The second photon, Ω_c varying from $2\pi \times 5.94$ MHz to $2\pi \times 23.79$ MHz by changing the 510 nm laser power, couples the Rydberg transition $|6P_{3/2}, F' = 5\rangle \to |nD_{5/2}\rangle$, with the frequency scanning through the Rydberg state. The autoionization experiment is performed in a standard cesium MOT with a temperature of $\sim$100 μK and a peak atomic density of $\sim 10^{10}$ cm^{-3}, measured by the shadow imaging method. Rydberg atoms, $|nD_{5/2}\rangle$, are prepared with a two-photon excitation of cold ground atoms. The two lasers are frequency stabilized using a high finesse optical cavity with 1.5 GHz FSR and 15,000 fineness. The 852 and 510 nm beams, with respective waists of 80 μm and 40 μm, are overlapped in a counter propagating geometry, thus yielding a cylindrical excitation region at the MOT center, see Figure 1b. The free ions and field ionized Rydberg ions are detected with an MCP detector, which has detection efficiency of about 10%. The detected ion signals are amplified with an amplifier and analyzed with a boxcar integrator (SRS-250) and then recorded with a computer. Before measurements, we first calibrate the MCP ion detection system with two shadow images taken before and after the laser excitation. From the difference in the two shadow images, we obtain the amount of Rydberg excitation and therefore the gain factor of the MCP detector. The excitation region is surrounded by three pairs of field-compensation electrodes, which allow us to reduce stray electric fields via Stark spectroscopy, corresponding to a stray field less than 30 mV/cm. According to the experimental timing shown in Figure 1c, in each experimental cycle, after turning off the MOT beams, we apply a two-photon pulse of 4 μs for the Rydberg excitation. Before the ramped pulse, we apply an interaction time t_D, allowing for investigating the autoionization of $nD_{5/2}$ Rydberg atoms.

In Figure 2, we present the TOF signals of the $37D_{5/2}$ Rydberg state with the ionization field value E_{ion} lower (red upper line) and higher (black lower line) than the ionization threshold E_{thres} ($E_{thres} \simeq 401.86$ V/cm), which is defined as the threshold electric field for ionizing $37D_{5/2}$ Rydberg atoms. The TOF spectrum with the field $E_{ion} > E_{thres}$ displays two peaks at the beginning marked with the blue square, see an enlargement in the inset of the Figure 2. The first narrow peak at 0.5 μs mainly comes from the autoionization ion signals, whereas the second broad peak at about 1.0 μs is attributed to the field ionization of the laser-excited $37D_{5/2}$ Rydberg atoms. The signals in the middle of the two peaks probably come from the high-lying Rydberg state produced due to the interaction. The small peak of the TOF spectrum of the field $E_{ion} = 118.85$ V/cm (much less than E_{thres}), see red upper line of Figure 2, provides the evidence that the first peak in the TOF is attributed to the autoionization signals. In order to avoid the effect of the $37D_{5/2}$ and high-lying Rydberg state, we set electric field $E_{ion} = 265.14$ V/cm to measure free ion signals.
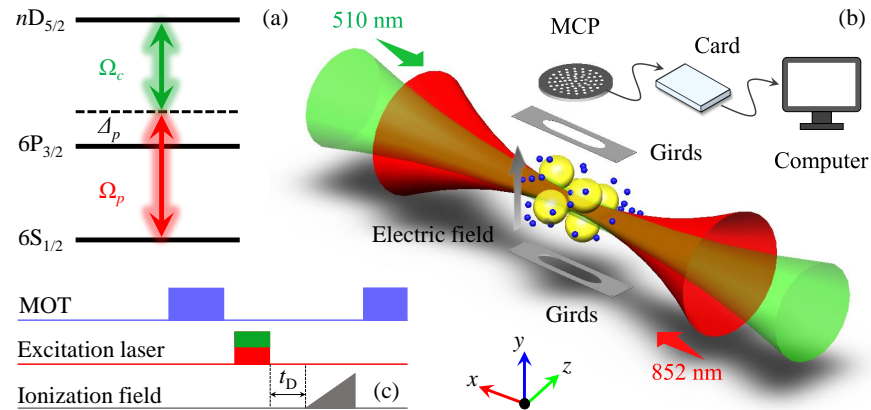
Figure 1. (**a**) Two-photon excitation diagram. The first photon, Ω_p, drives the lower transition, $|6S_{1/2}, F = 4\rangle \rightarrow |6P_{3/2}, F' = 5\rangle$, and its frequency is blue shifted $\Delta_p/2\pi$ = 360 MHz from the state $|6P_{3/2}, F' = 5\rangle$ using a double-pass acousto-optic modulator (AOM). The second photon, Ω_c, couples the Rydberg transition $|6P_{3/2}, F' = 5\rangle \rightarrow |nD_{5/2}\rangle$. (**b**) Sketch of an experimental setup. The coupling laser λ_c = 510 nm and probe laser λ_p = 852 nm are overlapped in the MOT center to excite ground atoms (small blue balls) to Rydberg states (large yellow balls). Free ions due to the autoionization are detected with the MCP detector and recorded with a computer. (**c**) Experimental timing. After switching off MOT beams, the two-photon excitation lasers are turned on to excite cesium ground atoms to the Rydberg state. A ramped electric field is finally applied to ionize the Rydberg atoms after interaction time t_D and drive free ions and Rydberg ions to the MCP detector. The rising time of the ramped field is 3 μs, and the peak value is defined as E_{ion}.
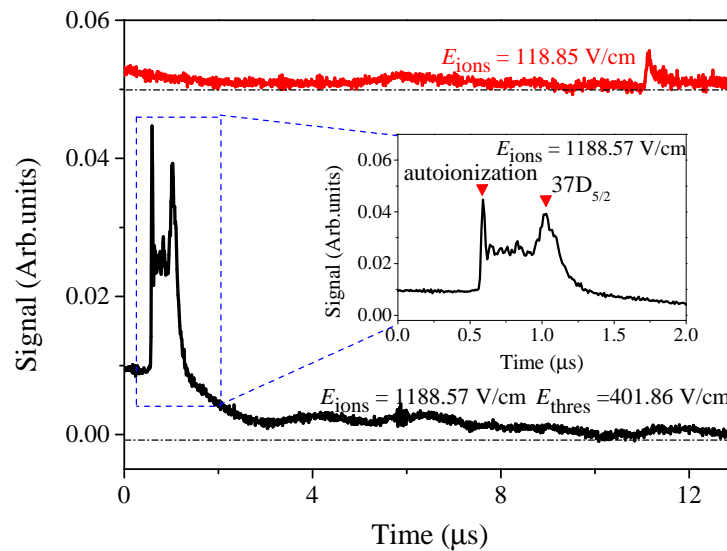
Figure 2. Time of flight (TOF) of the two-photon spectroscopy for the laser excitation to $37D_{5/2}$ Rydberg state. The red upper line displays the TOF spectrum for the field $E_{ion} < E_{thres}$ (the baseline of the red curve is offset to discern the signals.) The black lower line represents the TOF spectrum for the field $E_{ion} > E_{thres}$. The ionization threshold value E_{thres} of the $37D_{5/2}$ Rydberg state is 401.86 V/cm. The inset is an enlargement of the signals in the blue dashed area.

3. Autoionization Mechanism Analysis

The autoionization mechanism of Rydberg atoms may be caused by the following processes. The first is the penning ionization which comes from the collision of two Rydberg atoms at an attractive interaction potential. The process can be written as [15]:

$$Ryd(n) + Ryd(n) = Ryd(n^{'}) + ion + e^{-}, \qquad (1)$$
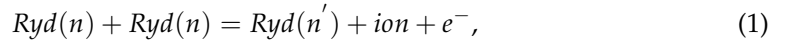
where $Ryd(n)$ represents the Rydberg atom with the principal quantum number n, the Rydberg pair collide with each other by the attractive interaction, one Rydberg atom is ionized and the other Rydberg atom is de-excited to a quantum state with a smaller principal quantum number, $n^{'}$, and the ionization cross sections are typically very large. For our experiment, the penning ionization has a negligible effect because the $37D_{5/2}$ pair displays a repulsive interaction potential. We calculate the long-range interaction potentials of the $37D_{5/2}$ pair for $|M| = 0$–5, where M $= m_{j1} + m_{j2}$, m_{j1} and m_{j2} are the magnetic quantum numbers of atom 1 and 2, respectively. The interaction potentials are shown in Figure 3a, which shows that all $|M|$ components display a repulsive interaction at the atomic density used in this work. The second is associative ionization which leads to the formation of the molecular ions. It is a short-range process depending on the overlap of the wave function. The ionization probability is usually related to the initial state n and the distance R between the two Rydberg atoms. In our experiment, the atomic density is $\sim 10^{10}$ cm^{-3}, which is insufficient to form molecules, so associative ionization is not the main mechanism for the formation of autoionization in this work.

The third is the ionization process induced by the blackbody radiation (BBR) at room temperature. The BBR-induced ionization is a complex process, which mainly includes two processes [23]: (i) the direct photoionization of initially prepared Rydberg atoms by absorbing *BBR* photons, which can be calculated by [23]

$$W_{BBR} = A_L \frac{11500T}{n_{eff}^{7/3}} [cos(\Delta_L^+ + \frac{\pi}{6})^2 + cos(\Delta_L^- - \frac{\pi}{6})^2] ln[\frac{1}{1 - exp(-\frac{157890}{Tn_{eff}^2})}](s^{-1}). \qquad (2)$$

Here, A_L is a scaling coefficient, which depends on the angular quantum number L and the alkali metal atoms, such as for Cs nD, $A_L = 0.35$. T is temperature, n_{eff} is effective quantum number, $\Delta_L^+ = \pi(\mu_L$-$\mu_{L+1})$, $\Delta_L^- = \pi(\mu_{L-1}$-$\mu_L)$, μ_{L-1}, μ_L and μ_{L+1} correspond to the quantum defects of the $L-1$, L and $L+1$ states, respectively. (ii) BBR-induced redistribution [24] to nearby Rydberg states and then ionization due to the BBR photonionization and the attractive interaction. At room temperature T, $\kappa T > \hbar \omega$ (κ, $\hbar$ and ω correspond to the Boltzmann constant, the Planck constant and the transition frequency, respectively), BBR photons of low-frequency microwave (MW) fields can provide successive energies to couple nearby Rydberg states. Therefore, BBR can cause not only the direct photoionization of the initially populated Rydberg levels, but also the transition between neighboring Rydberg states, thus leading to population redistribution [24]. For our experiment in the MOT at room temperature $T = 300$ K, we calculate BBR-induced decay rates of the $37D_{5/2}$ state to nearby states $37D_{5/2} \rightarrow n^{'}P_{3/2}$, as shown in Figure 3b. It is seen that the transition of $37D_{5/2} \rightarrow 39P_{3/2}$ plays an important role due to the largest decay rate of about 9000 s^{-1}. The redistributed $n^{'}P_{3/2}$ states may be further ionized by the BBR or the attractive interaction between the initial $nD_{5/2}$ and $n^{'}P_{3/2}$ states.
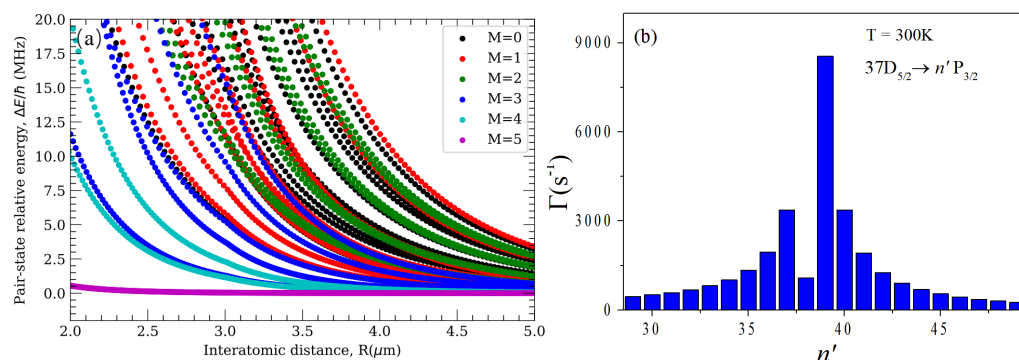
Figure 3. (**a**) The calculated interaction potential of $37D_{5/2}$ pair for $|M|$ = 0–5, indicating that the interaction is anisotropic for different $|M|$, where M = $m_{j1} + m_{j2}$, m_{j1} and m_{j2} are the magnetic quantum numbers of atom 1 and 2, respectively. At the Rydberg atomic density of ∼10^9 in this work, the interaction curves display repulsive potentials. (**b**) Calculations of the BBR-induced decay rates of $37D_{5/2} \rightarrow n'P_{3/2}$ transitions at T = 300 K. The transition of $37D_{5/2} \rightarrow 39P_{3/2}$ has the largest decay rate of ∼9000 s^{-1}.

4. Results and Discussion

In Figure 4a, we present the TOF spectra of autoionization signals for the laser excitation to the $37D_{5/2}$ Rydberg state with the indicated delay times, t_D, and the fixed Rydberg atomic density ρ = 2.96 × 10^9 cm^{-3}. For the curve of t_D = 0, in the bottom panel of Figure 4a, the TOF signals present a sharp narrow ionization signal, which is produced due to the direct photoionization of the initially prepared Rydberg atoms by absorbing BBR photons, as discussed in the last section, and the calculated BBR photoionization rate is W_{BBR} = 345 s^{-1}. The BBR photoionization process is assumed to occur during the Rydberg excitation, and the resultant BBR ions are accelerated to the MCP detector, forming the narrow signals when we apply a weak field for detecting. When we increase the delay time t_D, the autoionization signals show an increase and broadening, and the TOF signals move to a later time, see the middle and upper curves of Figure 4a. We attribute the increase in and broadening of the signals at a longer delay time t_D to the fact that (i) the BBR-induced transitions predominantly populate the neighboring Rydberg states, see Figure 3b, (ii) these BBR-populated states can be ionized either by the BBR or by the attractive interaction between the initially prepared nD state and the BBR-populated $n'P$ states.
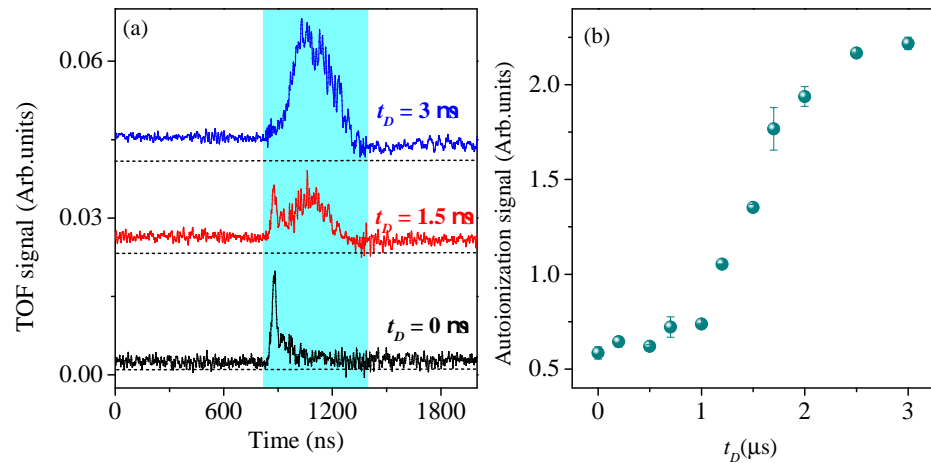
Figure 4. (**a**) Measured TOF spectra of autoionization signals for laser excitation to $37D_{5/2}$ Rydberg state with the indicated delay time t_D and the fixed Rydberg atomic density $\rho = 2.96 \times 10^9$ cm^{-3}. The cyan region marks the boxcar gate. The ramped field $E_{ion} \lesssim E_{thres}$. The zero point is the beginning of the ramped field. (**b**) Measurements of the autoionization signals of $37D_{5/2}$ Rydberg state as the function of delay time t_D. The data display the average of 100 measurements at the two-photon resonance.

In order to investigate the evolution of the ion signals, we measure all ion signals in the cyan gate of Figure 4a by a boxcar integrator (SRS-250) for the different delay times. Figure 4b presents the signals as a function of t_D with the Rydberg density of $\rho = 2.96 \times 10^9$ cm^{-3}. As we expect, the ion signals are very small for $t_D < 1$ µs, which is because the ionization signals are mainly caused by BBR-induced ionization. The ion signals display a fast increase at 1 µs $\lesssim t_D \lesssim 2$ µs, and the ion signals reach a maximum value at $t_D \simeq 3$ µs. The fast increase and tending to the maximum of ion signals after $t_D \sim 1$ µ are mainly due to the spontaneous evolution of cold Rydberg atoms into ultracold plasma, which is described by Robinson et al. [17].

The formation mechanism of plasma from Rydberg gases was analyzed in [7,17]. Rydberg atoms were ionized by the BBR and by collisions between Rydberg atoms after laser excitation. The resultant electrons leave the MOT quickly, while the ions stay at the MOT position, which attracts and traps the electrons, making them collide with the remaining Rydberg atoms, leading to the rapid avalanche ionization and formation of the plasma. The rapidly increased ions have strong Coulomb interactions that lead to the broadening of TOF spectra, see the upper curve in Figure 4a. To verify the evolution process we observed in Figure 4b, we have done more measurements for a different Rydberg atomic density that is changed by varying the power of the second excitation laser (510 nm laser). In Figure 5a, we display similar measurements as in Figure 4b but for the indicated Rydberg atomic density $\rho = 2.96 \times 10^9$ cm^{-3} (black squares), 1.93×10^9 cm^{-3} (red cycles), 1.46×10^9 cm^{-3} (blue triangles) and 7.40×10^8 cm^{-3} (purple diamonds). From Figure 5a, it is seen that the evolution of the Rydberg atoms strongly depends on the Rydberg atomic density: (i) initial ion signals at $t_D = 0$ linearly increase with the Rydberg density, see Figure 5b, which displays that the autoionization at $t_D = 0$ is the single-body process. (ii) The threshold time of the rapid avalanche also depends on the atomic density, and the larger the Rydberg density is, the shorter the threshold time of the rapid avalanche is. (iii) The maximum ion number increases with the atomic density. When the atomic density is less than 10^9, for example, in the measurement of the $\rho = 7.40 \times 10^8$ cm^{-3} case, the observed ion signals are very small and almost unchanged when we increase the delay time. It is found, from Figure 5, that the initial autoionization is the single-body process mainly due to the BBR-induced ionization, and the dynmaic evolution is the many-body process attributed to the collective collisions. For the case of the lower Rydberg density, the evolution caused by collision has a negligible effect, therefore we do not observe

the evolution process. In all, the BBR-induced ionization and redistribution at a nearby Rydberg state have an important role in the autoionization and evolution of the Rydberg $37D_{5/2}$ state, which is significant for investigating the collision between Rydberg atoms and many-body physics.
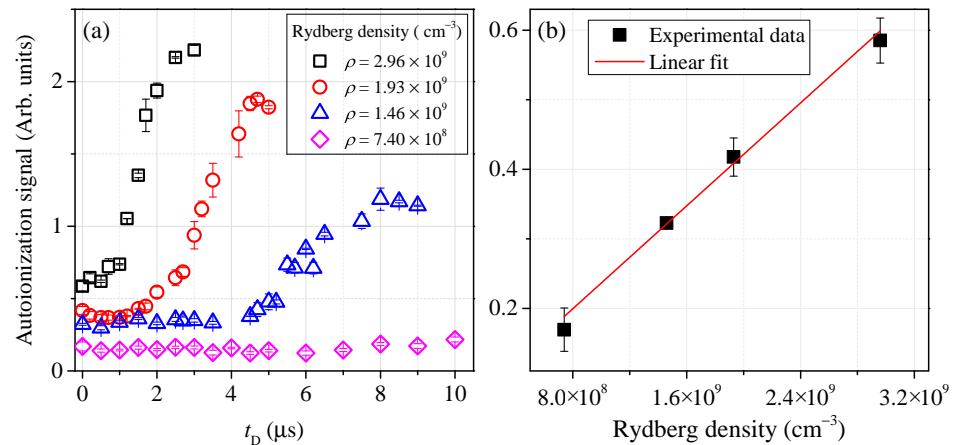
Figure 5. (**a**) Measured ion signals as a function of t_D for an indicated Rydberg atomic density. (**b**) Measured autoionization signals at $t_D = 0$ as a function of Rydberg atomic density.

5. Conclusions

In conclusion, $37D_{5/2}$ Rydberg atoms were excited with the two-photon excitation in a standard cesium MOT and ion signals due to the autoionization are detected with the MCP detector. We analyze the autoionization mechanism of Rydberg atoms, including the penning ionization, the associative ionization and the autoionization induced by the room temperature BBR. It is found that the initial ionization of $37D_{5/2}$ Rydberg atoms is mostly attributed to the BBR. The BBR-induced transition to the nearby Rydberg states that leads to the further BBR photoionization and dipole interaction has an important role in the further evolution of Rydberg atoms. The investigation of the dependence of the autoionization process on the Rydberg atomic density reveals that the Rydberg density has effects on the initial ion signals but also the evolution of the plasma. Our work plays a significant role in investigating the collision between Rydberg atoms and many-body physics.

Author Contributions: Conceptualization, J.Z.; methodology, J.Z.; software, J.B.; validation, Y.J. and L.H.; formal analysis, J.B.; investigation, Y.J. and L.H.; data curation, Y.J.; writing—original draft preparation, L.H. and J.F.; writing—review and editing, J.Z. and S.J.; visualization, Y.J.; supervision, J.Z.; project administration, J.Z.; funding acquisition, J.Z. All authors have read and agreed to the published version of the manuscript.

Institutional Review Board Statement: Not applicable.

Informed Consent Statement: Not applicable.

Data Availability Statement: The data presented in this study are available on request from the corresponding author.

Conflicts of Interest: The authors declare no conflict of interest.

References

1. Gallagher, T.F. *Rydberg Atoms*, 3rd ed.; Cambridge University Press: New York, NY, USA, 1994; pp. 1–9.
2. Tong, D.; Farooqi, S.M.; Stanojevic, J.; Krishnan, S.; Zhang, Y.P.; Côté, R.; Eyler, E.E.; Gould, P.L. Local blockade of Rydberg excitation in an ultracold gas. *Phys. Rev. Lett.* **2004**, *93*, 063001. [CrossRef] [PubMed]

3.　Urban, U.; Johnson, T.A.; Henage, T.; Isenhower, L.; Yavuz, D.D.; Walker, T.G.; Saffman, M. Observation of Rydberg blockade between two atoms. *Nat. Phys.* **2009**, *5*, 110–114. [CrossRef]

4.　Mourachko, I.; Comparat, D.A.; Tomasi, F.D.; Fioretti, A.; Nosbaum, P.; Akulin, V.M.; Pillet, P. Many-Body Effects in a Frozen Rydberg Gas. *Phys. Rev. Lett.* **1998**, *80*, 253–256. [CrossRef]

5.　Carroll, T.J.; Sunder, S.; Noel, M.W. Many-body interactions in a sample of ultracold Rydberg atoms with varying dimensions and densities. *Phys. Rev. A* **2006**, *73*, 032725. [CrossRef]

6.　Walz-Flannigan, A.; Guest, J.R.; Choi, J.-H.; Raithel, G. Cold-Rydberg-gas dynamics. *Phys. Rev. A* **2004**, *69*, 063405. [CrossRef]

7.　Li, W.; Noel, M.W.; Robinson, M.P.; Tanner, P.J.; Gallagher, T.F.; Comparat, D.; Tolra, B.L.; Vanhaecke, N.; Vogt, T.; Zahzam, N.; et al. A. Evolution dynamics of a dense frozen Rydberg gas to plasma. *Phys. Rev. A* **2004**, *70*, 042713. [CrossRef]

8.　Li, W.; Tanner, P.J.; Gallagher, T.F. Dipole-Dipole Excitation and Ionization in an Ultracold Gas of Rydberg Atoms. *Phys. Rev. Lett.* **2005**, *94*, 173001. [CrossRef]

9.　Amthor, T.; Reetz-Lamou, M.; Giese, C.; Weidemüller, M. Modeling many-particle mechanical effects of an interacting Rydberg gas. *Phys. Rev. A* **2007**, *76*, 054702. [CrossRef]

10.　Weimer, H.; M*ü*ller, M.; Lesanovsky, I.; Zoller, P.; Büchler, H.P. A Rydberg quantum simulator. *Nat. Phys.* **2010**, *6*, 382–388. [CrossRef]

11.　Browaeys, A.; Lahaye, T. Many-body physics with individually controlled Rydberg atoms. *Nat. Phys.* **2020**, *16*, 132–142. [CrossRef]

12.　Lukin, M.D.; Fleischhauer, M.; Cote, R.; Duan, L.M.; Jaksch, D.; Cirac, J.I.; Zoller, P. Dipole Blockade and Quantum Information Processing in Mesoscopic Atomic Ensembles. *Phys. Rev. Lett.* **2001**, *87*, 037901. [CrossRef] [PubMed]

13.　Jaksch, D.; Cirac, J.I.; Zoller, P.; Rolston, S.L.; Côté, R.; Lukin, M.D. Fast Quantum Gates for Neutral Atoms. *Phys. Rev. Lett.* **2000**, *85*, 2208. [CrossRef] [PubMed]

14.　Bloom, B.J.; Nicholson, T.L.; Williams, J.R.; Campbell, S.L.; Bishof, M.; Zhang, X.; Zhang, W.; Bromley, S.L.; Ye, J. An optical lattice clock with accuracy and stability at the 10^{-18} level. *Nature* **2014**, *506*, 71–75. [CrossRef] [PubMed]

15.　Amthor, T.; Denskat, J.; Giese, C.; Bezuglov, N.N.; Ekers, A.; Cederbaum, L.S.; Weidemüller, M. Autoionization of an ultracold Rydberg gas through resonant dipole coupling. *Eur. Phys. J. D* **2009**, *53*, 329–335. [CrossRef]

16.　Efimov, D.D.; Miculis, K.; Bezuglov, N.N.; Ekers, A. Strong enhancement of Penning ionization for asymmetric atom pairs in cold Rydberg gases: The Tom and Jerry effect. *J. Phys. B At. Mol. Opt. Phys.* **2016**, *49*, 125302. [CrossRef]

17.　Robinson, M.P.; Tolra, B.L.; Noel, M.W.; Gallagher, T.F.; Pillet, P. Spontaneous Evolution of Rydberg Atoms into an Ultracold Plasma. *Phys. Rev. Lett.* **2000**, *85*, 4466. [CrossRef]

18.　Olson, R. Ionization Cross Sections for Rydberg-Atom-Rydberg-Atom Collisions. *Phys. Rev. Lett.* **1979**, *43*, 126. [CrossRef]

19.　Yoshida, S.; Burgdörfer, J.; Fields, G.; Brienza, R.; Dunning, F.B. Giant cross sections for L changing in Rydberg-Rydberg collisions. *Phys. Rev. A* **2020**, *102*, 022805. [CrossRef]

20.　Hahn, Y. Density dependence of molecular autoionization in a cold gas. *J. Phys. B At. Mol. Opt. Phys* **2000**, *33*, L655. [CrossRef]

21.　Gawlas, K.; Hogan, S.D. Rydberg-state ionization dynamics and tunnel ionization rates in strong electric fields. *Phys. Rev. A* **2019**, *99*, 013421. [CrossRef]

22.　Stecker, M.; Noldg, R.; Steinert, L.M.; Grimmel, J.; Petrosyan, D.; Fortgh, J.; Günther, A. Controlling the Dipole Blockade and Ionization Rate of Rydberg Atoms in Strong Electric Fields. *Phys. Rev. Lett.* **2020**, *125*, 103602. [CrossRef] [PubMed]

23.　Beterov, I.I.; Tretyakov, D.B.; Ryabtsev, I.I.; Entin, V.M.; Ekers, A.; Bezuglov, N.N. Ionization of Rydberg atoms by blackbody radiation. *New J. Phys.* **2009**, *11*, 013052. [CrossRef]

24.　Miculis, K.; Beterov, I.I.; Bezuglov, N.N.; Ryabtsev, I.I.; Tretyakov, D.B.; Ekers, A.; Klucharev, A.N. Collisional and thermal ionization of sodium Rydberg atoms: II. Theory for nS, nP and nD states with n = 5–25. *J. Phys. B At. Mol. Opt. Phys* **2005**, *38*, 1811. [CrossRef]